Journal of Solid State Chemistry 184 (2011) 843–847

Contents lists available at ScienceDirect

Journal of Solid State Chemistry

journal homepage: www.elsevier.com/locate/jssc

Determining the structure of tetragonal Y_2WO_6 and the site occupation of Eu^{3+} dopant

Jinping Huang*, Jun Xu, Hexing Li, Hongshan Luo, Xibin Yu, Yikang Li

Department of Chemistry, Shanghai Normal University, 100 Guilin Road, Xuhui District, Shanghai 200234, PR China

ARTICLE INFO

Article history:
Received 2 November 2010
Received in revised form
27 January 2011
Accepted 11 February 2011
Available online 20 February 2011

Keywords:
Rietveld refinement
Structure determination
Powder diffraction
Site occupation
Long wavelength ultraviolet excitation

ABSTRACT

The compound Y_2WO_6 is prepared by solid state reaction at 750 °C using sodium chloride as mineralizer. Its structure is solved by ab-initio methods from X-ray powder diffraction data. This low temperature phase of yttrium tungstate crystallizes in tetragonal space group $P4/nmm$ (No. 129), $Z=2$, $a=5.2596(2)$ Å, $c=8.4158(4)$ Å. The tungsten atoms in the structure adopt an unusual [WO_6] distorted cubes coordination, connecting [YO_6] distorted cubes with oxygen vacancies at the O_2 layers while other yttrium ions Y_2 form [YO_8] cube coordination. Y^{3+} ions occupy two crystallographic sites of $2c$ (C_{4v} symmetry) and $2a$ (D_{2d} symmetry) in the Y_2WO_6 host lattice. With Eu^{3+} ions doped, the high resolution emission spectrum of Y_2WO_6:Eu^{3+} suggests that Eu^{3+} partly substituted for Y^{3+} in these two sites. The result of the Rietveld structure refinement shows that the Eu^{3+} dopants preferentially enter the $2a$ site. The uniform cube coordination environment of Eu^{3+} ions with the identical eight Eu–O bond lengths is proposed to be responsible for the intense excitation of long wavelength ultraviolet at 466–535 nm.

1. Introduction

Rare earth tungstates $mLn_2O_3 \cdot nWO_3$ constitute a large family of material with versatile solid-state properties which depend on the structure, rare earth element and tungsten oxidation state[1–3]. Initial interest in luminescence of rare earth tungstates derived from their structure relationship with scheelite [4], which suggests efficient luminescence properties [5,6]. The needs for new optical materials of high quantum yield and long wavelength ultraviolet-excited advance the field of rare earth tungstates for luminescence materials [7]. Whatever as host matrices doped with photoactive ions [8,9] or as intrinsic phosphors [10], rare earth tungstates show the merits of high stability, brightness and long wavelength ultraviolet-excitation [11]. The luminescence properties are strongly dependent on the local chemical environment of activator ion, such as coordination number, site symmetry and bond character, which ultimately depend on the crystal structure. Doubtless, detailed information of the structure features for rare earth tungstates would help in the interpretation for their optical spectra and mechanisms of site-to-site energy transfer. However, in the synthesis of rare earth tungstates, the product of single crystal or pure phase is often unavailable, which directly results in that many reported compositions lack structural detail or were not fully characterized in the $mLn_2O_3 \cdot nWO_3$ system [12,13]. Up to now, yttrium tungstates with the composition Y_2WO_6 has fallen mainly into several crystallographic forms: monoclinic $P2_1/m$ (No. 11), orthorhombic $P2_12_12_1$ (No. 19), etc., which were prepared by solid state reaction above 1600 K [14–18].

Here we report the synthesis and structure determination of a novel low temperature polymorph Y_2WO_6. The luminescence properties of Eu^{3+}-activated Y_2WO_6 are also investigated. It is well known that Eu^{3+}-activated emission spectrum is sensitive to the coordination environment of Eu^{3+}, and the intensity is strongly influenced by the crystallographic site, where the cations are located. Yttrium tungstates as the important luminescence matrixes, when with Eu^{3+} doped, Eu^{3+} cations would partly occupy the crystallographic sites of Y^{3+} [18–20]. The structure information of Y_2WO_6 is expected to be probed by the luminescence performance of Eu^{3+}-activated.

2. Experimental section

The compound Y_2WO_6 was prepared by solid-state reaction of pure oxides. The oxides were weighed according to stoichiometric amount of Y_2O_3, WO_3 and NaCl with a molar ratio of 1:1:0.25. They were grounded together in an agate mortar. The NaCl acts as the mineralizer. The mixed composition was calcined at 750 °C for 10 h in a porcelain crucible. The product was washed several times with distilled water to remove the impurity and then desiccated at 110 °C. The Eu^{3+}-activated fluorescent sample Y_2WO_6:Eu was prepared by the same method with a molar ratio of Y_2O_3, Eu_2O_3, WO_3 and NaCl 0.9:0.1:1:0.25.

* Corresponding author. Fax: +86 21 6432 2270.
E-mail addresses: hjinping@shnu.edu.cn (J. Huang), xujun16@163.com (J. Xu), hexing-li@shnu.edu.cn (H. Li), lhs@shnu.edu.cn (H. Luo), xibinyu@shnu.edu.cn (X. Yu), liyikang1973@sina.com (Y. Li).

0022-4596/$ - see front matter © 2011 Elsevier Inc. All rights reserved.
doi:10.1016/j.jssc.2011.02.015

The composition of the final product was inspected using scaning electron microscope (SEM, JSM-6360LV) equipped with an energy-dispersive spectrum (EDS, Falcon). Quantitative analysis was separately carried out on several crystalline particles, and the mean value was adopted.

X-ray diffraction patterns were collected on a Bragg–Brentano diffractometer (Rigaku D/Max-2000) with monochromatic Cu$K\alpha$ radiation ($\lambda=0.15418$ nm) of graphite curve monochromator. The X-ray diffraction data for structure determination and refinement was collected from [9–130°, 2θ], with the step length of 0.02 (2θ) and counting times of 40 s per step.

The low-resolution excitation and emission spectra were measured at room temperature by Varian Cary-Eclipse 500 spectrofluorometer with a 60 W xenon lamp as excitation source. The high-resolution excitation and emission spectra were measured at room temperature by Horiba Jy Fluorolog-3 spectrofluorometer with a 450 W steady state xenon lamp as excitation source. The spectral slit width is 0.3/0.2 nm, the scan step is 0.2 nm. The emission spectra were corrected for detection and optical spectral response of the spectrofluorometer, and the excitation spectra were weighed for the spectral distribution of the lamp intensity using a photodiode reference detector. In order to ensure a quantitative comparison between the emission intensity of different spectra, the measurements were done consecutively and all the experimental conditions (optical setup, focalization point and illuminated cross-section, sample holder and emission, excitation slits width, etc.) were kept constant.

3. Results and discussion

3.1. Sample preparation and characterization

A series of synthesis around the nominal composition (Y_2O_3:WO_3:NaCl=1:1:0.25) have been carried out to improve the purity of the product (S1-1 and S1-2 in support information). However, all the alteration cannot eliminate impurities from the products, only modifying a little of the height or width of the diffractograms. The optimal ratio of the reactants Y_2O_3:WO_3:NaCl=1:1:0.25 was determined, with which the molar ratio of Y to W is 20.1(1):10.0(5) in the product inspected by Energy-dispersive spectrum (EDS). In the synthesis, sodium chloride was used as mineralizer, which alters the reaction temperature and the structure symmetry, ultimately leading to the formation of the objective compound. Without sodium chloride the final product is a mixture of multiphase and the tetragonal Y_2WO_6 is unavailable. After the reaction completed, NaCl was washed off. Composition inspection of the final product by EDS did not find elements Na and Cl.

The X-ray diffraction pattern (S2 in support information) was rather similar to the compound $Y_6W_2O_{15}$ previously reported by Borchardt [18] in the JCPDS reference 15-0473. $Y_6W_2O_{15}$ was considered as a metastable phase between 750 and 1000 °C and inseparable from other phases. However, this result contradicts to the EDS composition analysis of Y: W=2:1.

3.2. Crystal structure determination

Fig. 1 shows the Bragg positions of the diffraction lines and the Rietveld refinement result of powder X-ray diffractogram for the title compound. The first 20 peak positions of the main phase Y_2WO_6 were indexed using program ITO [21], TREOR [22], DICVOL [23], McMaille [24]. Only McMaille gives the solution of tetragonal cell with $a=5.262$ Å, $c=8.421$ Å ($R_p=0.105$, FOM=382.76) [24]. Then, the cell is confirmed by Le Bail refinement [25,26] through the Fullprof software [27]. In the process of indexing, two impure phases were found in the diffraction pattern. Automatic search using software Jade 6.0 indicates that the powder pattern contained small amount of Y_2O_3 (JCPDS No. 43-1036). In addition, the remaining peaks with 2θ at 28.4, 30.3, etc. are attributed to another impurity $WO_{2.92}$ (JCPDS No. 30–1387). Through the systematic absences observed from the powder data, and with the help of the Chekcell software [28], the most likely space group was $P4/nmm$ (No. 129) and $P4/n$ (No. 85). We select each of them to establish the structure model of Y_2WO_6. Now that $P4/nmm$ and $P4/n$ have the same extinction conditions ($hk0$: $h+k=2n$) and ($h00$: $h=2n$), the trial-and-error method was used to test the suitability of the space group. First, the $P4/nmm$ was tested. The extracted intensities from the diffraction pattern were used for attempting the structure solution by direct methods embedded in the Sir2008 software [29] and by the reverse Monte Carlo and pseudo simulated annealing code embedded in the ESPOIR software [30]. The partial structure model was given by SIR2008 software. We retrieved Y1, Y2 and W atoms with ESPOIR software, the O1 is obvious on the Fourier map at special position 8j. Then, we retrieved Y1, Y2, W and O1 atoms again, the O2 also appears on the Fourier map away from W, Y1 and Y2 with the distances of 1.97, 2.37 and 2.44, respectively. We suggest O2 at $x=1/4$, $y=0.008$, $z=0.555$ half occupied at special position 8i, which may mean a disorder on the last O atom, leading to [WO_6] and [YO_6] the distorted cubes with a statistical half occupancy oxygen at the O2 layers. Others [YO_8] form cubes (Fig. 2). However, for the $P4/n$ (No. 85) we cannot get the acceptable structure model after several attempts with varying the parameters, especially when decreasing the minimum normalized structure amplitude (Emin) to generate phases. Direct or Patterson methods failed to provide a satisfying starting model as well. So, the space group $P4/nmm$ (No. 129) has the most probability.

Then, Fullprof program was used for the structure refinements [31]. The pseudo-Voigt function was used for approximation of the diffraction profiles. The refined instrumental and structural parameters were: zero shifts, scale factors, background

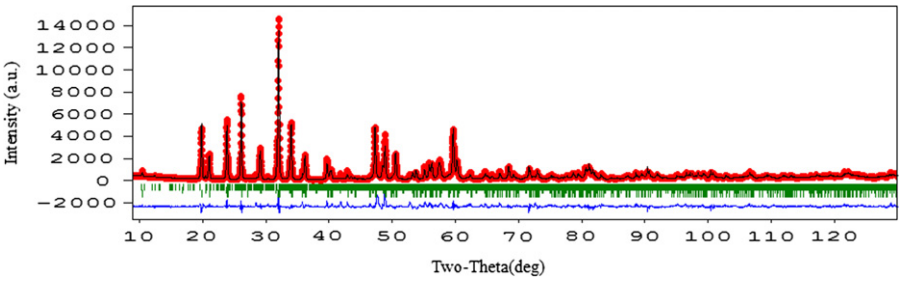

Fig. 1. Bragg positions of the diffraction lines and the Rietveld refinement result. Red dots represent the observed data, black lines the calculated data, and ticks the peak position of $WO_{2.92}$ (above), Y_2O_3 (middle) and Y_2WO_6 (below). The bottom line in blue shows the difference between observed and calculated data. (For interpretation of the references to color in this figure legend, the reader is referred to the web version of this article.)

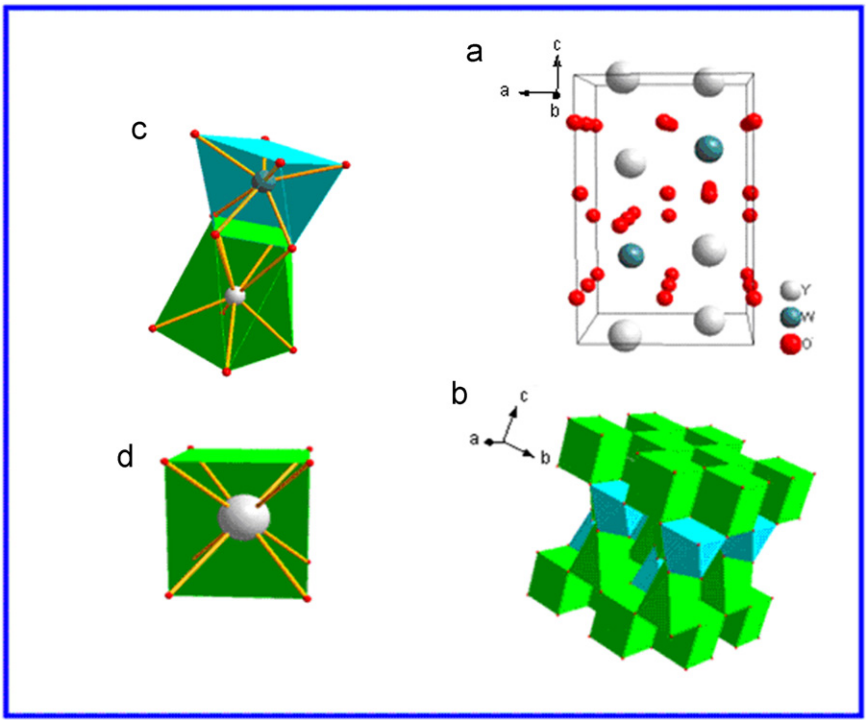

Fig. 2. Crystal structure of Y_2WO_6: (a) The unit cell of Y_2WO_6; (b) Schematic of [YO_8] cube (green) connecting [WO_6] (blue) and [YO_6] (green) distorted cubes with each other; (c) the distorted cube coordination of Y1 and W; and (d) the cube coordination environment of Y2. (For interpretation of the references to color in this figure legend, the reader is referred to the web version of this article.)

Table 1
Crystallographic parameters of Y_2WO_6 from Rietveld refinement [a]

Atom	Site	*x*	*y*	*z*	B_{iso} (Å^2)	Occ
Y1	2*c*	0.25	0.25	0.3348(7)	1.90	1
Y2	2*a*	0.25	0.75	0	1.58	1
W	2*c*	0.25	0.25	0.7242(2)	0.77	1
O1	8*j*	0.0003(6)	0.0003(6)	0.8258(8)	1.79	1
O2 [b]	8*i*	0.25	0.0007(7)	0.5597(9)	1.33	0.5

[a] X-ray diffraction pattern: 145 reflections, R_p=15.2%, R_{wp}=20.3%, R_{Bragg}=8.12%, R_F=5.86%. Space group *P*4/*nmm* (No. 129), *a*=5.2596(2) Å, *c*=8.4158(4) Å, *Z*=2, calculated density=5.2596 g/cm^{-3}.
[b] Half-occupied site.

Table 2
Selected interatomic distances found in Y_2WO_6.

Atom 1	Atom 2	Distance (Å)
Y1	O2	2.302(1)
Y1	O1	2.301(2)
Y2	O1	2.368(2)
W	O2	1.910(1)
W	O1	2.044(2)

Table 3
Calculated bond valence and atomic coordination numbers (CN) for Y_2WO_6

Atom	CN	BV sum (σ)
Y1	6	2.79(5)
Y2	8	3.11(2)
W	6	4.88(5)
O1	4	1.95(3)
O2	2	1.49(1)

B=0.37, R_0 ($Y^{3+}-O^{2-}$)=2.019 Å and R_0 ($W^{6+}-O^{2-}$)=1.917 Å.

parameters, lattice parameters, line profile parameters, atomic positional parameters, individual isotropic displacement parameters and site occupations. The Rietveld refinement details for Y_2WO_6 are shown in Table 1. The final fitting factors are R_p=15.2%, R_{wp}=20.3%, R_{Bragg}=8.12% and R_F=5.86%. The minor phase $WO_{2.92}$ is not easy to refine because the phase fraction is little and the peak overlapping, which may contribute to this high R_{wp} value. Considering the existence of the impure phase as mentioned above, this refinement result is satisfactory. The phase fraction of Rietveld refinement Y_2WO_6 is 99.07%, Y_2O_3 0.92% and $WO_{2.92}$ 0.01%, then confirmed by the simulation with Fullprof. The coefficient to calculate the weight percentage of the phase (ATZ) of Y_2WO_6, Y_2O_3 and $WO_{2.92}$ are 915.32, 1616 and 2434, respectively. The atomic parameters including isotropic temperature factor, atomic coordinates and occupation factor are gathered in Table 1. The atomic coordination numbers and the interatomic distances are shown in Table 2.

Based on the crystal structure of Y_2WO_6, bond valence (BV) calculation was performed directly by the program VaList [32], the program Bond-Str [27] was used to import data. Using the Brown–Altermatt empirical expression: valence=$\Sigma\exp(R_0-d)/B$ with *B*=0.37 Å [33]. The values used by VaList program were for $Y^{3+}-O^{2-}$ R_0=2.019 Å and for $W^{6+}-O^{2-}$ R_0=1.917 Å [34]. The results of the bond valence calculations for each atom type give values around the expected +3, +6, −2 for yttrium, tungsten and oxygen atom, respectively (see Table 3). We can mention that the discrepancies between calculated and theoretical values are similar to the structural analysis of $La_{18}W_{10}O_{57}$ [35,36]. The small coordination number of O2 may contribute the small BV value obtained. The two oxygen atoms O1 and O2 are bonded to tungsten atoms and have a statistical half occupancy that could introduce local distortion. Furthermore, the long oxygen–cation distances of *d* (W–O1)=2.044(2) Å and *d* (Y1−O2)=2.302(1) Å may also cause the smaller bond valence values of W and O2. From the bond distance in Table 2, it can be clearly seen that the

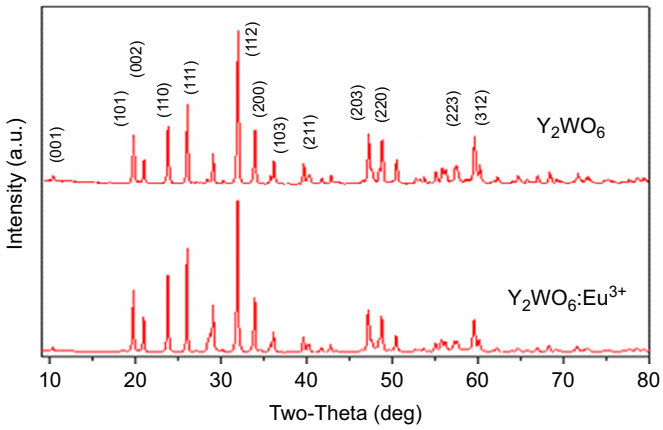

Fig. 3. X-ray powder diffraction pattern of Y_2WO_6:Eu^{3+} in comparison with Y_2WO_6 host lattice.

W atom adopts distorted cubes coordination through two O2 atoms connecting Y1 in [YO6] distorted cubes with oxygen vacancies at the O2 layers. Meanwhile, two O1 atoms of [WO6] distorted cubes connect Y2 of [YO8] cube by sharing an edge.

3.3. Luminescence property and site occupation

The X-ray diffraction patterns of Eu^{3+}-doped Y_2WO_6 is shown in Fig. 3. It can be observed that the diffraction peaks coincide well with Y_2WO_6 host lattice. No other impurity phases were found. Furthermore, no obvious shifting of the diffraction peaks was observed when Eu^{3+} ions doped into the host lattice. The lattice parameters of Y_2WO_6:Eu^{3+} is calculated as $a=5.2659(3)$ and $c=8.4294(3)$ Å, larger than the ones of Y_2WO_6. Because when Eu^{3+} substitutes for Y^{3+} in Y_2WO_6, the larger Eu^{3+} ions (ionic radius of Eu^{3+} (CN6) 0.095, Y^{3+} (CN6) 0.090 nm) have enlarged the dimensions of the Y_2WO_6 host lattice.

The excitation spectrum of Y_2WO_6:Eu^{3+} monitored at $^5D_0 \rightarrow {}^7F_2$ lines is depicted in Fig. 4. The spectrum consists of a broadband peaking at 288 nm assigned to the $O \rightarrow Eu^{3+}$ charge transfer (LMCT) bands and of characteristic Eu^{3+} sharp lines ascribed to intra-$4f^6$ transitions within the Eu^{3+} $4f^6$ electronic configuration. The relative intensity of $^7F_0 \rightarrow {}^5D_2$ excitation at 466 and 535 nm presents an unusual increase. It is contrary to the usual intensity distribution of Eu^{3+} excitation spectrum, in which the 395 nm excitation is more intensive than 466 nm. This phenomenon was also observed on $EuKNaTaO_5$ [37], in which Eu^{3+} cation is located in cube coordination environment with eight identical Eu–O distances (2.4476 Å). This uniform coordination site of Eu^{3+} may bring on the intense excitation of long wavelength ultraviolet at 466 and 535 nm.

For Y_2WO_6:Eu^{3+}, under various excitation wavelengths, the hypersensitive transition $^5D_0 \rightarrow {}^7F_2$ of Eu^{3+} ions at 612 nm displays prominent emission intensity, while the magnetic dipole transition $^5D_0 \rightarrow {}^7F_1$ emission at 590 nm is forbidden. This spectral intensity distribution is in accordance with the well-known behavior of Eu^{3+} location at a non-inversion symmetry site. Moreover, the emission lines from the *f–f* transition of Eu^{3+} in crystalline sites are generally quite sharp. With changing the excitation from the LMCT band to direct excitation into the $4f^6$ levels ($^5L_6$ 395 nm, or $^5D_2$ 466 nm), the full width at half-maximum (FWHM) and Stark components remain unaltered.

We try to assign the Eu^{3+} excitation and emission features with the local coordination site. Y_2WO_6 lattice has two local sites available for Y^{3+} cations, namely 2*c* site (C_{4v} symmetry) and 2*a* (D_{2d} symmetry) site in Wyckoff notation (shown in Fig. 2c and d). When Eu^{3+} ions doped, it partly substituted for Y^{3+} and may randomly occupy the two crystallographic sites [20]. Whichever

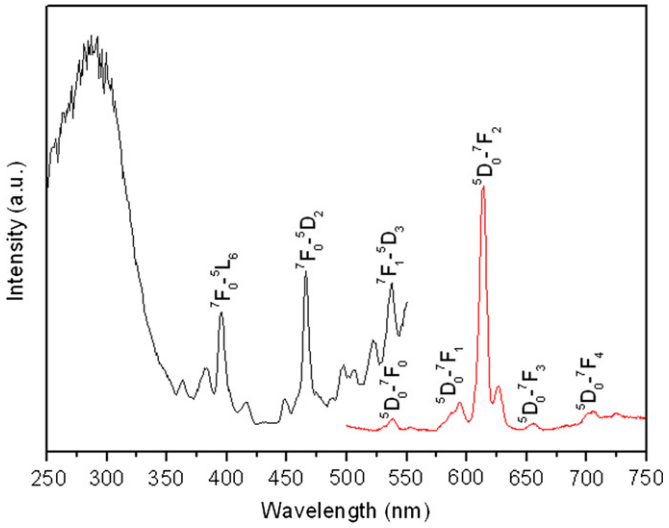

Fig. 4. Excitation and emission spectra of Y_2WO_6:Eu^{3+}.

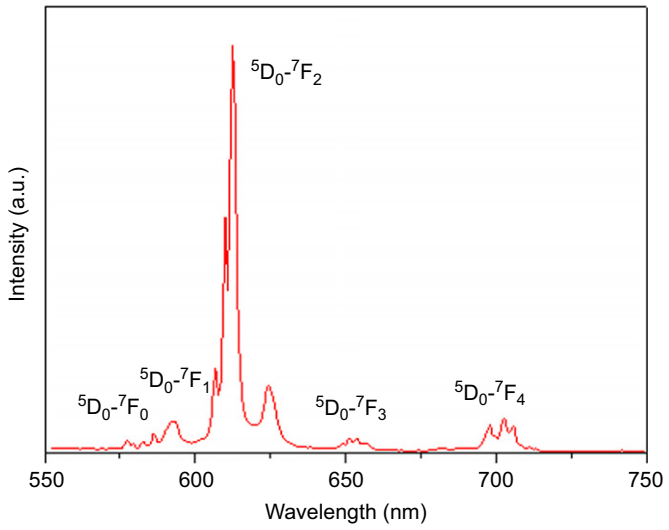

Fig. 5. High resolution emission spectra of Y_2WO_6:Eu^{3+}. Four lines of $^5D_0 \rightarrow {}^7F_2$ transition represent more than one crystallographic site being occupied by Eu^{3+}.

Eu^{3+} ions reside in, it allows the hypersensitive electric dipole emission of $^5D_0 \rightarrow {}^7F_2$ under UV excitation because both the C_{4v} and D_{2d} sites lack inversion symmetry. From the high-revolution emission spectrum in Fig. 5, it can be observed that the $^5D_0 \rightarrow {}^7F_0$ shows one line, the $^5D_0 \rightarrow {}^7F_1$ transition four lines and $^5D_0 \rightarrow {}^7F_2$ transition four lines. It suggests that there is more than one crystallographic site being occupied by Eu^{3+} in the structure of Y_2WO_6 [38–40]. For the transition of Eu^{3+} ions in one site, the maximum number of lines amounts to one, two and two, respectively. In addition, these crystallographic sites lack inversion symmetry, otherwise, the $^5D_0 \rightarrow {}^7F_2$ transitions would be strictly forbidden. The structure of Y_2WO_6 accounts for the emission spectrum.

The site occupation of Eu^{3+} ions is predicted by X-ray diffraction analysis. The final fitting factors are $R_p=15.2\%$, $R_{wp}=20.3\%$, $R_{Bragg}=7.91\%$ and $R_F=5.76\%$. After refining site occupations of Y1 and Y2, the Rietveld refinement step results in $2(c)$:nY1$=0.123(2)$ and $2(a)$:nY2$=0.117(3)$. Considering the fully occupied site (nY$=0.125$) and doping amount of Eu^{3+} ions (Eu:Y$=0.1$:0.9), the site occupancy of Eu^{3+} in Y1 position is 20%, while in Y2 position is 80%. This calculation result suggests that Eu^{3+} prefers to occupy the Y2 position of 2*a* with D_{2d} symmetry. Rietveld refinement gives the bond distance Y2–O1$=2.368(2)$ Å which is longer than both R_0 value

Y–O=2.019 and d (Y1–O1)=2.301(2) Å, d (Y1–O2)=2.302(1) Å. According to the valence bond theory [41], the more the electron cloud overlapped, the stronger the bond energy. So the longer bond distance of Y2–O1 results in the weaker bond energy, which facilitates Eu^{3+} ions to substitute Y2 and to populate in the cube coordination sites. This coordination environment with eight uniform Eu–O bond lengths endows intense excitation at 466 and 535 nm of Y_2WO_6:Eu^{3+}. Although the other 20% Eu^{3+} ions adopt distorted cubes coordination of Eu1–O, it does not alter the basic emission features of Y_2WO_6:Eu^{3+}. The uniform local structure around the dopants Eu^{3+} give rise to the sharp and strong luminescence spectrum of Y_2WO_6:Eu^{3+} under different excitation wavelengths.

Conclusions

The tetragonal yttrium tungstate has been prepared by solid state reaction at 750 °C. The energy-dispersive spectrum (EDS) demonstrates the stoichiometric fraction of yttrium to tungsten is 2:1. Sodium chloride acts the role of both mineralizer and structure capping agent, which reduces the reaction temperature and alters the structure symmetry, ultimately leading to the formation of tetragonal Y_2WO_6. The crystal structure of Y_2WO_6 has been determined from X-ray powder diffraction data. When Eu^{3+} ion doped, it partly substituted for Y^{3+} and may occupy the two crystallographic sites. The site occupation of Eu^{3+} is determined by the analysis of the emission spectrum and the Rietveld refinement from XRD data. The result indicates that Eu^{3+} strongly prefers to occupy the Y2 position of 2a with D_{2d} symmetry, which endows uniform eight bond length of Eu–O. This undistorted cube coordination environment is proposed to be responsible for the prominent long wavelength excitation at 466 and 535 nm of Y_2WO_6:Eu^{3+}.

Acknowledgments

We would like to thank Prof. Lv Guanglie in Chemistry Department of Zhejiang University for his beneficial discussion on this research, and MDI technical support in helping to analyze the space group.

Appendix A. Supplementary material

Supplementary data associated with this article can be found in the online version at doi:10.1016/j.jssc.2011.02.015.

References

[1] N. Kim, J.F. Stebbins, Chemistry of Materials 21 (2) (2009) 309–315.
[2] P. Lacorre, E. Goutenoire, O. Bohnke, R. Retoux, Y. Laligant, Nature 404 (2000) 856–858.
[3] D. Marrero-Lopez, J. Pena-Martinez, J.C. Ruiz-Morales, P. Nunez, Journal of Solid State Chemistry 181 (2) (2008) 253–262.
[4] L.G. Van Uitert, The Journal of Chemical Physics 37 (5) (1962) 981.
[5] G. Blasse, A. Bril, The Journal of Chemical Physics 45 (7) (1966) 2350–2355.
[6] G. Blasse, G.P.M. van den Heuvel, J.J.A. van Hesteren, Journal of Solid State Chemistry 21 (2) (1977) 99–103.
[7] B. Moine, G. Bizarri, Optical Materials 28 (1–2) (2006) 58–63.
[8] L. Macalik, P.E. Tomaszewski, R. Lisiecki, J. Hanuza, Journal of Solid State Chemistry 181 (10) (2008) 2591–2600.
[9] Q. Shao, H. Li, K. Wu, Y. Dong, J. Jiang, Journal of Luminescence 129 (8) (2009) 879–883.
[10] J. Huang, H. Luo, X. Yu, Y. Li, W. Zou, Journal of Luminescence 128 (4) (2008) 589–594.
[11] S. Neeraj, N. Kijima, A.K. Cheetham, Chemical Physics Letters 387 (1–3) (2004) 2–6.
[12] M. Yoshimura, A. Rouanet, Materials Research Bulletin 11 (2) (1976) 151–158.
[13] J. Huang, H. Luo, P. Zhou, X. Yu, Y. Li, Journal of Luminescence 126 (2) (2007) 881–885.
[14] M. Yoshimura, E. Sibieude, A. Rouanet, M. Foex, Journal of Solid State Chemistry 16 (3-4) (1976) 219–232.
[15] O. Beaury, M. Faucher, G.T. de Sagey, P. Caro, Materials Research Bulletin 13 (9) (1978) 953–957.
[16] J. Wang, Z. Zhang, J. Zhao, H. Chen, X. Yang, Y. Tao, Y. Huang, Journal of Material Chemistry 20 (2010) 10894–10900.
[17] O. Beaury, M. Faucher, G.T.D.E. Sagey, Acta Crystallographica Section B 37 (1981) 1166.
[18] H.J. Borchardt, Inorganic Chemistry 2 (1) (1963) 170–173.
[19] G. Concas, G. Spano, E. Zych, J. Trojan-Piegza, Journal of Physics, Condensed Matter 17 (17) (2005) 2597–2604.
[20] M.M.A.D.B. Antic, Journal of Physics: Condensed Matter 9 (1997) 365–374.
[21] J.W. Visser, Journal of Applied Crystallography 2 (3) (1969) 89–95.
[22] P.E. Werner, L. Eriksson, M. Westdahl, Journal of Applied Crystallography 18 (5) (1985) 367–370.
[23] A. Boultif, D. Lou E R, Journal of Applied Crystallography 37 (5) (2004) 724–731.
[24] A.Le Bail, Powder Diffraction 19 (3) (2004) 249.
[25] A. Le Bail, H. Duroy, J.L. Fourquet, Materials Research Bulletin 23 (3) (1988) 447–452.
[26] A.L. Bail, Powder Diffraction 20 (4) (2005) 316–326.
[27] J. Rodriguez-Carvajal, Toulouse, France 1990, , 127.
[28] CHEKCELL is written by J. Laugier, B. Bochu, and distributed free from the CCP14 website: 〈http://www.ccp14.ac.uk/tutorial/lmgp/〉.
[29] M.C. Burla, R. Caliandro, M. Camalli, B. Carrozzini, G.L. Cascarano, L. De Caro, C. Giacovazzo, G. Polidori, D. Siliqi, R. Spagna, Journal of Applied Crystallography 40 (3) (2007) 609–613.
[30] A.LeBail, ProgramEspoir3.5,〈http://sdpd.univ-lemans.fr/sppd/espoir/, 2000〉.
[31] H.M. Rietveld, Journal of Applied Crystallography 2 (2) (1969) 65–71.
[32] Wills, A.S, VaList, Program available from www.ccp14.ac.uk/tutorial/lmgp/.
[33] I.D. Brown, U.D. Altermatt, Acta Crystallographica Section B 41 (4) (1985) 244–247.
[34] N.E. Brese, M. O'Keeffe, Acta Crystallographica Section B 47 (2) (1991) 192–197.
[35] L.H. Brixner, H.Y. Chen, C.M. Foris, Journal of Solid State Chemistry 44 (1) (1982) 99–107.
[36] M.L.N. Chambrier, A. Le Bail, S.P. Kodjikian, E. Suard, F.O. Goutenoire, Inorganic Chemistry 48 (14) (2009) 6566–6572.
[37] I.P. Roof, M.D. Smith, S. Park, H.Z. Loye, Journal of the American Chemical Society 131 (12) (2009) 4202–4203.
[38] S. Zhang, Chinese Journal of Luminescence 3 (1983) 18–23.
[39] G.S. Ofelt, The Journal of Chemical Physics 37 (3) (1962) 511.
[40] B. Judd, Physical Review 127 (3) (1962) 750–761.
[41] J.N. Murrel, S.F.T. Sons., The Chemical Bond., John Wiley & Sons, 1985.